General Analysis of Multiuser MIMO Systems With Regularized Zero-Forcing Precoding Under Spatially Correlated Rayleigh Fading Channels

Harsh Tataria*, Peter J. Smith†, Pawel A. Dmochowski*, Mansoor Shafi‡
* School of Engineering and Computer Science, Victoria University of Wellington, Wellington, New Zealand
† School of Mathematics and Statistics, Victoria University of Wellington, Wellington, New Zealand
‡ Spark New Zealand, Wellington, New Zealand
email:{harsh.tataria, pawel.dmochowski}@ecs.vuw.ac.nz, peter.smith@vuw.ac.nz, mansoor.shafi@spark.co.nz

***Abstract*—A general framework for the analysis of expected per-user signal-to-interference-plus-noise-ratio (SINR) of a multiuser multiple-input-multiple-output system is presented. Our analysis assumes spatially correlated Rayleigh fading channels with regularized zero-forcing precoding on the downlink. Unlike previous works, our analytical expressions are averaged over the eigenvalue densities of the complex Wishart distributed channel correlation matrix. To aid the derivation of the expected per-user SINR, we derive a closed-form expression for the joint density of two arbitrary eigenvalues of the complex Wishart matrix. In the high signal-to-noise-ratio (SNR) regime, with zero-forcing precoding, we derive analytical expressions to approximate the instantaneous per-user SNR and show that it is approximately gamma distributed. The generality of the approximations is validated with numerical results over a wide range of system dimensions, spatial correlation and SNR levels.**

I. Introduction

Multiuser multiple-input-multiple-output (MU-MIMO) systems have gained tremendous amounts of attention due to the multiplexing gains resulting from their ability to simultaneously serve a multiplicity of user terminals in the same time-frequency interval [1]. This has led to enhancements in spectral efficiency and bit error rate in the downlink [2]. The underlying channel for downlink MU-MIMO transmission is often referred to as the MIMO broadcast channel (MIMO-BC) [3]. The MIMO-BC suffers from inter-user interference, leading to a lower signal-to-interference-plus-noise-ratio (SINR) at a given user terminal. This has motivated the use of channel aware pre-processing techniques, such as spatial precoding at the base station (BS).

If the BS has channel knowledge, dirty-paper coding (DPC) is known to achieve the capacity of a Gaussian MIMO-BC [3]. However, DPC is a non-linear precoding technique with high complexity. In comparison, sub-optimal linear precoding methods have been identified more practical due to their lower complexity [4]. Moreover, with the introduction of large antenna arrays, the preponderance of serving antennas at the BS over the terminals has shown that linear precoding techniques, such as zero-forcing (ZF) beamforming can achieve up to 98% of the DPC capacity [5]. However, to compensate for noise inflation in the low signal-to-noise-ratio (SNR) regime, regularized zero-forcing (RZF) precoding was proposed [4]. In practice, as the deployment of large antenna arrays must be carried out in confined volumes, the adverse effects of spatial correlation on the per-user SINR and achievable rate will be inevitable, due to antenna elements residing in close proximity. Hence, analysis of MU-MIMO systems with spatial correlation is of greater significance in understanding the practically realizable gains [6].

Numerous works have theoretically characterized the performance of downlink MU-MIMO systems by means of SINR and sum-rate analysis (see [7, 8] and references therein). However, much of this work considers simple uncorrelated Rayleigh fading channels. The sum-rate performance of conventional and large MU-MIMO systems under spatially correlated channels with linear precoding and combining techniques was analyzed in [9, 10] and references therein. The effects of transmit spatial correlation with antenna coupling on the sum-rate performance has been studied in [6]. In [11, 12], pre-processing at the BS is specifically tailored for correlated channels to maximize the sum-rate performance. However, the focus of all the above has been on characterizing cell-wide performance, rather than performance on a per-user basis. Motivated by this, we analyze the expected per-user SINR performance via an eigenvalue decomposition of the Wishart distributed channel correlation matrix, where we consider averaging over the density of the respective eigenvalues. In doing so, we extend the results of [4] that only consider averaging over the isotropic eigenvector distribution for simplicity.

In particular, the contributions of the paper are as follows:

- We derive tight analytical expressions to approximate the expected per-user SINR with spatial correlation at the BS. Our expressions are averaged over the arbitrary eigenvalue densities of the complex Wishart channel correlation matrix. To the best of the authors' knowledge, such an analysis has not been carried out previously and was considered to be extremely difficult in [4].
- To aid the derivation of the expected signal and interference powers at a given terminal, we derive a closed-form expression for the previously unknown joint density of two arbitrary eigenvalues of the channel correlation matrix.
- At high SNRs, as RZF precoding converges to ZF precoding, we derive analytical expressions to approximate

the instantaneous per-user SNR. We demonstrate that the instantaneous per-user SNR approximately follows a gamma distribution and derive its parameters.
- The generality and tightness of the developed expressions is verified via numerical results with a wide-range of system dimensions, spatial correlation levels and SNRs in the system.

Notation: Boldface lower and upper case symbols represent vectors and matrices, respectively. $\boldsymbol{I}_M$ denotes the $M \times M$ identity matrix. The transpose, Hermitian transpose, inverse and trace operators are denoted by $(\cdot)^{\mathrm{T}}$, $(\cdot)^{\mathrm{H}}$, $(\cdot)^{-1}$ and $\mathrm{tr}\,(\cdot)$, respectively. We use $\boldsymbol{h} \sim \mathcal{CN}\left(\mu, \sigma^2\right)$ to denote a complex Gaussian distribution for $\boldsymbol{h}$, where each element of $\boldsymbol{h}$ has mean μ and variance σ^2. $||\cdot||_{\mathrm{F}}^2$ and $|\cdot|$ denote the Frobenius and scalar norms, while $\forall$ reads as "for all". $\mathbb{E}\,[\cdot]$, $\mathrm{Var}\,[\cdot]$, $\mathrm{per}\,(\cdot)$ and $\det\,(\cdot)$ represent statistical expectation, variance, sign of permutation and determinant operators, respectively.

II. System Model

A. Signal Model

We consider the downlink of a MU-MIMO system, where the BS is equipped with an array of M transmit antennas, serving K non-cooperative single antenna user terminals ($M \geq K$) in the same time-frequency interval. We assume narrow-band transmission and equal power allocation to each terminal. With perfect channel knowledge at the BS, the received signal at the k-th terminal can be written as

$$y_k = \sqrt{\frac{\beta_k}{\eta}} \boldsymbol{h}_k \boldsymbol{w}_k s_k + \sqrt{\frac{\beta_k}{\eta}} \sum_{\substack{i=1 \\ i \neq k}}^{K} \boldsymbol{h}_k \boldsymbol{w}_i s_i + z_k, \tag{1}$$

where β_k is the received power from the BS to the k-th terminal (discussed later in the text). We model the channel vectors, $\boldsymbol{h}_k$, as $\boldsymbol{h}_k = \boldsymbol{u}_k \sqrt{\boldsymbol{R}}$, where $\boldsymbol{u}_k \sim \mathcal{CN}\left(0, \boldsymbol{I}_M\right)$ is the fast-fading channel vector and $\boldsymbol{R}$ is a transmit correlation matrix. We postpone the discussion of the particular structure of $\boldsymbol{R}$ to Section V. However, we note the generality of the present channel model, as it allows us to consider any type of antenna correlation structure in $\boldsymbol{R}$. Although we consider the general case of MU-MIMO, the above model is of particular relevance for large antenna arrays, where strong antenna correlation may arise as a result of inadequate inter-element spacing or lack of multi-path diversity [13]. $\boldsymbol{w}_k$ is the $M \times 1$ un-normalized precoding vector from the BS to the k-th terminal and s_k is the data symbol desired for the k-th user, such that $\mathbb{E}\left[|s_k|^2\right] = 1$. Following [14], $\eta = ||\boldsymbol{W}||_{\mathrm{F}}^2 / K$ is the precoder normalization factor, such that the transmit power per-terminal is normalized to ε. $z_k \sim \mathcal{CN}\left(0, \sigma_k^2\right)$ models the effects of additive white Gaussian noise at the k-th terminal. The received power from the BS to the k-th terminal is modeled as in [15], where

$$\beta_k = \varepsilon \zeta \left(\frac{d_0}{d_k}\right)^{\alpha} \psi_k. \tag{2}$$

Here, ζ is a unit-less constant for geometric attenuation at a reference distance d_0, assuming far-field, omni-directional transmit antennas, d_k is the link distance from the BS to user k, α is the attenuation exponent and $\psi_k = 10^{(S_j \sigma_s / 10)}$ models the effects of shadow-fading with a log-normal distribution, where $S_j \sim \mathcal{N}\left(0, 1\right)$ and σ_s is the shadow-fading standard deviation. The corresponding value of each parameter has been chosen from [15] and tabulated in Section V. Finally, we refer to SNR as the ratio of the long term received power to the noise power at the receiver.

B. Downlink Precoding and Per-User SINR

In this study, we use RZF precoding to design the downlink precoding vectors. Here, $\boldsymbol{w}_k$ is the k-th column of the $M \times K$ precoding matrix, $\boldsymbol{W}$, defined as

$$\boldsymbol{W} \triangleq \left(\boldsymbol{H}^{\mathrm{H}} \boldsymbol{H} + \xi \boldsymbol{I}_M\right)^{-1} \boldsymbol{H}^{\mathrm{H}}, \tag{3}$$

where $\boldsymbol{H} \triangleq \left[\boldsymbol{h}_1^{\mathrm{T}}, \boldsymbol{h}_2^{\mathrm{T}}, \ldots, \boldsymbol{h}_K^{\mathrm{T}}\right]^{\mathrm{T}}$ is a $K \times M$ matrix composed by concatenating individual user channels. The constant $\xi = K/\mathrm{SNR} > 0$ denotes the regularization parameter and is chosen from [4] to maximize SINR at the receiver. The received signal in (1) can be translated into a received SINR for the k-th terminal and expressed as

$$\mathrm{SINR}_k = \frac{\frac{\beta_k}{\eta} |\boldsymbol{h}_k \boldsymbol{w}_k|^2}{\sigma_k^2 + \frac{\beta_k}{\eta} \sum\limits_{\substack{i=1 \\ i \neq k}}^{K} |\boldsymbol{h}_k \boldsymbol{w}_i|^2}. \tag{4}$$

III. Expected Per-User SINR Analysis

Following [16], the expected SINR for the k-th terminal can be approximated as

$$\mathbb{E}\left[\mathrm{SINR}_k\right] \approx \frac{\frac{\beta_k}{\tilde{\eta}} \mathbb{E}\left[|\boldsymbol{h}_k \boldsymbol{w}_k|^2\right]}{\sigma_k^2 + \frac{\beta_k}{\tilde{\eta}} \sum\limits_{\substack{i=1 \\ i \neq k}}^{K} \mathbb{E}\left[|\boldsymbol{h}_k \boldsymbol{w}_i|^2\right]}, \tag{5}$$

where $\tilde{\eta} = \mathbb{E}\left[\eta\right]$. In the following, the main technical results of the paper are presented, as we derive the expectations in (5) for the signal and interference powers, respectively. For the remainder of the paper, we denote $n = \max\left(M, K\right)$ and $m = \min\left(M, K\right)$, assuming $M \geq K$, as mentioned earlier in the text.

A. Expected Signal Power

By eigenvalue decomposition, we denote the complex Wishart distributed channel correlation matrix, $\boldsymbol{H}^{\mathrm{H}} \boldsymbol{H} = \boldsymbol{Q} \boldsymbol{\Lambda} \boldsymbol{Q}^{\mathrm{H}}$. Then, the expected value of the numerator in (5) is denoted by δ_k and can be written as [4]

$$\delta_k = \mathbb{E}\left[|\boldsymbol{h}_k \boldsymbol{w}_k|^2\right] = \mathbb{E}\left[\left(\sum_{i=1}^{m} \frac{\lambda_i}{\lambda_i + \xi} |q_{k,i}|^2\right)^2\right], \tag{6}$$

where λ_i is the i-th eigenvalue corresponding to the i-th diagonal entry in $\boldsymbol{\Lambda}$. $q_{k,i}$ denotes the entry of $\boldsymbol{Q}$ corresponding to the k-th row and i-th column. Using the fact that $\boldsymbol{Q}$ has an isotropic distribution, the expectation in (6) can be simplified by averaging over the entries of $\boldsymbol{Q}$, which yields [4]

$$\delta_k = \frac{1}{m\left(m+1\right)} \left\{ \mathbb{E}_{\lambda}\left[\left(\sum_{i=1}^{m} \frac{\lambda_i}{\lambda_i + \xi}\right)^2\right] + \mathbb{E}_{\lambda}\left[\sum_{i=1}^{m} \left(\frac{\lambda_i}{\lambda_i + \xi}\right)^2\right] \right\}. \tag{7}$$

The expectations in (7) can be further evaluated with respect to (w.r.t.) the density of the eigenvalues and are given in Theorems 1 and 3, respectively.

Theorem 1: If $\theta_1, \ldots, \theta_n$ are the n eigenvalues of $\boldsymbol{R}$, then the expected value of $\sum_{i=1}^{m} \frac{(\lambda_i)^{\bar{\mu}}}{(\lambda_i+\xi)^2}$, w.r.t. the eigenvalues of $\boldsymbol{H}^{\mathrm{H}}\boldsymbol{H}$ is given by

$$G_k^{(\bar{\mu})} = mL \sum_{l=1}^{m} \sum_{\substack{j=1 \\ j\neq l}}^{m} \mathcal{D}(l,j) \left[\left(\theta_{n-m+l}^{n-m-1} \Phi_2(n-m+l) \right) - \left(\sum_{p=1}^{n-m} \sum_{\substack{q=1 \\ q\neq p}}^{n-m} \left[\boldsymbol{\Psi}^{-1}\right]_{q,p} \theta_{n-m+l}^{q-1} \theta_p^{n-m-1} \Phi_2(p) \right) \right], \tag{8}$$

where $\left[\boldsymbol{\Psi}^{-1}\right]_{q,p}$ denotes the (q,p)-th entry of $\left[\boldsymbol{\Psi}^{-1}\right]$. The constant

$$L = \frac{\det(\boldsymbol{\Psi})}{m \prod_{q<p}^{n} (\theta_p - \theta_q) \prod_{p=1}^{m-1} p!}, \tag{9}$$

with $\boldsymbol{\Psi}$ being an $(n-m)\times(n-m)$ Vandermonde matrix

$$\boldsymbol{\Psi} = \begin{bmatrix} 1 & \theta_1 & \ldots & \theta_1^{n-m-1} \\ \vdots & \vdots & \ddots & \vdots \\ 1 & \theta_{n-m} & \ldots & \theta_{n-m}^{n-m-1} \end{bmatrix},$$

while $\mathcal{D}(l,j)$ is the (l,j)-th co-factor of the $m\times m$ matrix whose (p,q)-th entry equals

$$(q-1)! \left(\theta_{n-m+p}^{n-m+q-1} - \sum_{e=1}^{n-m} \sum_{f=1}^{n-m} \left[\boldsymbol{\Psi}^{-1}\right]_{e,f} \theta_{n-m+p}^{e-1} \theta_f^{n-m+q-1} \right).$$

$$\Phi_2(a) = \sum_{\gamma=0}^{\bar{\mu}} \binom{\bar{\mu}}{\gamma} (-\xi)^{\bar{\mu}-\gamma} e^{\xi/\theta_a} \int_{\xi}^{\infty} x^{\gamma-2} e^{-x} dx, \tag{10}$$

where $\bar{\mu} = 2 + j - 1$ and

$$\int_{\xi}^{\infty} x^{\gamma-2} e^{-x} dx = \begin{cases} -\mathrm{Ei}(1,\xi) + \frac{\mathrm{e}^{-\xi}}{\xi^2} \; ; \gamma = 0 \\ \mathrm{Ei}(1,\xi) \quad ; \gamma = 1 \\ \Gamma(\gamma-1,\xi) \quad ; \gamma \geq 2, \end{cases} \tag{11}$$

with $\mathrm{Ei}(\cdot,\cdot)$ and $\Gamma(\cdot,\cdot)$ being the generalized exponential integral and incomplete gamma functions, respectively.

Proof: See Appendix A.

Theorem 2: When $\theta_1, \ldots, \theta_n$ are the n eigenvalues of $\boldsymbol{R}$, the joint density of *any* arbitrary pair of eigenvalues, (λ_1, λ_2), of $\boldsymbol{H}^{\mathrm{H}}\boldsymbol{H}$ is given by

$$f_0(\lambda_1,\lambda_2) = T(n-2)! \sum_{i=0}^{m-1} \sum_{\substack{l=0 \\ l\neq i}}^{m-1} (-1)^{i+l-p(i,l)} \sum_{o=1}^{m} (-1)^{o-1} \theta_o^{n-m-1} \lambda_1^i e^{-\lambda_1/\theta_o} \sum_{\substack{p=1 \\ p\neq o}}^{m} (-1)^{p-p(0)} \theta_p^{n-m-1} \lambda_2^l e^{-\lambda_2/\theta_p} \boldsymbol{\Theta}, \tag{12}$$

where

$$T = \frac{1}{\prod_{j=1}^{m} j! \boldsymbol{\Delta}} \text{ with } \boldsymbol{\Delta} = \begin{bmatrix} 1 & \theta_1 & \ldots & \theta_1^{n-1} \\ \vdots & \vdots & \ddots & \vdots \\ 1 & \theta_n & \ldots & \theta_n^{n-1} \end{bmatrix}. \tag{13}$$

Furthermore,

$$p(i,l) = \begin{cases} 0\,;\, i > l \\ 1\,;\, i \leq l, \end{cases} \quad p(o) = \begin{cases} 0\,;\, p > o \\ 1\,;\, p \leq o, \end{cases} \tag{14}$$

and $\boldsymbol{\Theta} = \det(\boldsymbol{\Delta}_{o;p} \boldsymbol{\Xi}_{o,p;i,l})$ with

$$\boldsymbol{\Xi} = \begin{bmatrix} 1 & \ldots & \theta_1^{n-m-1} & \theta_1^{n-m-1} e^{-\lambda_1/\theta_1} & \ldots \\ \vdots & & \vdots & \vdots & \\ 1 & \ldots & \theta_n^{n-m-1} & \theta_n^{n-m-1} e^{-\lambda_1/\theta_n} & \ldots \end{bmatrix}.$$

Note that $\boldsymbol{\Delta}_{o;p}$ and $\boldsymbol{\Xi}_{o,p;i,l}$ denote the reduced versions of $\boldsymbol{\Delta}$ with row o and column p removed and $\boldsymbol{\Xi}$ with rows o,p and columns i,l removed.

Proof: See Appendix B.

Remark 1: The result derived in Theorem 2 is used to compute the expected per-user SINR and has general applicability for analysis involving complex Wishart matrices with spatially correlated channels. It is also worth mentioning that the result is scalable to arbitrary numbers of transmit and receive antennas and allows us to analyze the higher order statistics of spatially correlated channels, further used to characterize the capacity distribution of such channels [17].

Theorem 3: When $\theta_1, \ldots, \theta_n$ are the n eigenvalues of $\boldsymbol{R}$, the expected value of $\left(\sum_{i=1}^{m} \frac{\lambda_i}{\lambda_i+\xi}\right)^2$ w.r.t. the eigenvalues of $\boldsymbol{H}^{\mathrm{H}}\boldsymbol{H}$ is given by,

$$D_k = G_k^{(2)} + m(m-1)T(n-2)! \sum_{i=0}^{m-1} \sum_{\substack{l=0 \\ l\neq i}}^{m-1} \sum_{o=1}^{m} \sum_{\substack{p=1 \\ p\neq o}}^{m} (-1)^{i+l-p(i,l)} (-1)^{o-1} \theta_o^{n-m-1} (-1)^{p-p(o)} \boldsymbol{\Theta}\, \Phi_1(o) \Phi_1(p), \tag{15}$$

where T, $p(i,l)$, $p(o)$ and $\boldsymbol{\Theta}$ are as defined in (13) and (14), respectively.

$$\Phi_1(o) = \sum_{\gamma=0}^{\hat{\mu}} \binom{\hat{\mu}}{\gamma} (-\xi)^{\hat{\mu}-\gamma} e^{\xi/\theta_o} \int_{\xi}^{\infty} x^{\gamma-1} e^{-x} dx, \tag{16}$$

where $\hat{\mu} = i+1$ and the integral is a special case of the integral in (11). $\Phi_1(p)$ has the same form as $\Phi_1(o)$ with $\hat{\mu} = l+1$.

Proof: See Appendix C.

Using (8) and (15), we can write the expected signal power at the k-th terminal as

$$\delta_k = \frac{D_k + G_k^{(2)}}{m(m+1)}. \tag{17}$$

The expected value of the precoder normalization parameter, $\tilde{\eta}$, can also be expressed w.r.t. the eigenvalue densities of $\boldsymbol{H}^{\mathrm{H}}\boldsymbol{H}$ as

$$\tilde{\eta} = \frac{1}{m}\mathbb{E}\left[||\boldsymbol{W}||_{\mathrm{F}}^2\right] = \frac{1}{m}\mathbb{E}_{\lambda}\left[\sum_{i=1}^{m} \frac{\lambda_i}{(\lambda_i+\alpha)^2}\right] = \frac{1}{m} G_k^{(1)}. \tag{18}$$

B. Expected Interference Power

From [4], we note that the total expected received power (desired and interference) at the k-th user terminal can be written as

$$\varphi_k = \frac{\mathbb{E}\left[||\boldsymbol{H}\boldsymbol{W}||_{\mathrm{F}}^2\right]}{m} = \frac{1}{m}\left[\mathbb{E}_{\lambda}\left\{\sum_{i=1}^{m}\left(\frac{\lambda_i}{\lambda_i+\alpha}\right)^2\right\}\right] = \frac{1}{m} G_k^{(2)}. \tag{19}$$

From this, the expected interference power at the k-th terminal can be defined as ι_k, the difference between the total expected received power and the expected signal power [4]. Hence,

$$\iota_k = \varphi_k - \delta_k = \frac{1}{m} G_k^{(2)} - \frac{D_k + G_k^{(2)}}{m\,(m+1)}. \tag{20}$$

From (17), (18) and (20), the expected SINR at user k can now be written as a function of δ_k, $\tilde{\eta}$ and ι_k as

$$\mathbb{E}\left[\mathrm{SINR}_k\right] \approx \frac{\frac{\beta_k}{\tilde{\eta}} \delta_k}{\sigma_k^2 + \frac{\beta_k}{\tilde{\eta}} \left(m-1\right) \iota_k}. \tag{21}$$

Remark 2: As well as being robust to changes in system dimensions, the derived results can also be applied to other system types, such as heterogeneous cellular networks, where a hierarchy of BSs may be present. In such cases, the additional presence of inter-cellular interference can be characterized in the same manner as shown above [18]. Furthermore, the analysis is also applicable to other channel distributions, such as Ricean fading, as shown in [19].

The accuracy of the derived analytical expression in (21) is demonstrated in Section V. In the following section, we consider the high SNR regime, in which we approximate the instantaneous per-user RZF SINR with ZF precoding.

IV. High SNR Approximation

It is well known that the performance of RZF precoding converges to ZF precoding in the limit of increasing SNR [4]. This is due to the fact that the regularization constant, $\xi \to 0$, as SNR $\to \infty$. The per-user SINR remains as defined in (4). However, as ZF completely eliminates MU interference, the SINR at the k-th terminal becomes an SNR defined as

$$\mathrm{SNR}_k^{\mathrm{ZF}} = \frac{\beta_k}{\sigma_k^2 \,\mathrm{tr}\left\{\left(\boldsymbol{H}^{\mathrm{H}}\boldsymbol{H}\right)^{-1}\right\}}. \tag{22}$$

In the case of uncorrelated Rayleigh fading channels, it is well known that the SNR of classic ZF exactly follows a Chi-squared distribution [20]. As the Chi-squared distribution is a special case of the gamma distribution, we are motivated to approximate $\mathrm{SNR}_k^{\mathrm{ZF}}$ with a gamma distribution in this more general situation. In order to use this approximation, the shape and scale parameters of the gamma distribution have to be derived, as shown in Theorem 4.

Theorem 4: If $\mathrm{SNR}_k^{\mathrm{ZF}}$ follows a gamma distribution, then $\omega = \mathrm{tr}\left\{\left(\boldsymbol{H}^{\mathrm{H}}\boldsymbol{H}\right)^{-1}\right\}$ is an inverse gamma random variable, denoted as $\Gamma\left(\varrho, \chi\right)^{-1}$, where the shape and scale parameters

$$\varrho = 2 + \frac{\mathbb{E}\left[\omega\right]^2}{\mathrm{Var}\left[\omega\right]} \text{ and } \chi = \frac{\beta_k}{\left(1 + \frac{\mathbb{E}\left[\omega\right]^2}{\mathrm{Var}\left[\omega\right]}\right) \mathbb{E}\left[\omega\right]}, \tag{23}$$

are found from (47) and (48) in Appendix D using the method of moments.

Proof: See Appendix D.

We evaluate the accuracy of Theorem 4 in the following section.

V. Numerical Results

Unless otherwise specified, the simulation and analytical results are generated with the parameters specified in Table I. We

Parameter	Value
Cell type & radius	Circular & 100 meters (m)
User distribution	uniform w.r.t. cell area
Reference distance, d_0	1 m
Unit-less geometric attenuation constant, ζ	31.54 dB
Attenuation exponent, α	3.7
Shadowing standard deviation, σ_s	8 dB

TABLE I
System Parameters

model the presence of spatial correlation at the BS assuming fixed physical spacing with a Kronecker model, where the correlation assumed constant for each terminal follows an exponential distribution with the correlation matrix, $\boldsymbol{R}_{ij} = \rho^{|i-j|}$ for $i, j \in \{1, \ldots, n\}$ [21]. The Rayleigh assumptions include rich scattering around the BS and here it is reasonable to assume constant correlation per-terminal, dependent only on the array structure. Naturally, $\rho = 0$ results in an uncorrelated Rayleigh fading channel and conversely $\rho = 1$ represents a fully correlated channel, comparable to having a co-located antenna array at the BS. For each subsequent result, the noise power at each terminal was set to unity and 10^4 Monte-Carlo simulations were carried out.

First, the accuracy of the proposed expected per-user SINR approximation in (21) is examined. Fig. 1 illustrates the expected per-user SINR as a function of SNR for a system with $M = 7$ and 10 with $K = 6$. As can be readily observed, the proposed approximation remains sufficiently accurate for the entire SNR range of interest. In addition, we observe that increasing ρ to 0.9 has an adverse effect on the expected per-user SINR, as an increase in the level of correlation reduces the spatially usable degrees of freedom, resulting in a loss in the per-user SINR. An alternative interpretation of this could be that reducing the spatial degrees of freedom at the BS increases the level of inter-user interference, leading to a lower per-user SINR. The analytical approximations are seen to remain tight even with an extremely high level of spatial correlation in $\rho = 0.9$ for both $M = 7, 10$ cases, respectively. This fact is also evident in Fig. 2, where the expected per-user SINR is shown to exponentially degrade as a function of ρ for $M = 7$ and 10 at SNR $= 10$ dB. The derived analytical approximations are seen to remain very accurate for the entire range of ρ.

We now study the impact of increasing M on expected SINR with K remaining fixed. Fig. 3 shows the expected per-user SINR as a function of M with $K = 6$ at SNR $= 10$ dB. While the expected SINR increases, its diminishing returns can be observed with increasing M. This is a result of the channels to multiple users becoming asymptotically pairwise orthogonal, as the typical angular spacing between any two terminals is greater than the angular Rayleigh resolution of the transmit array [1]. In-turn this reduces the inner product of any two channel vectors to zero. This has famously been recognized as convergence to favorable propagation conditions in the large MIMO system literature [1]. We can also observe that with increasing levels of spatial correlation, the rate of saturation also increases. For all cases, the derived expressions

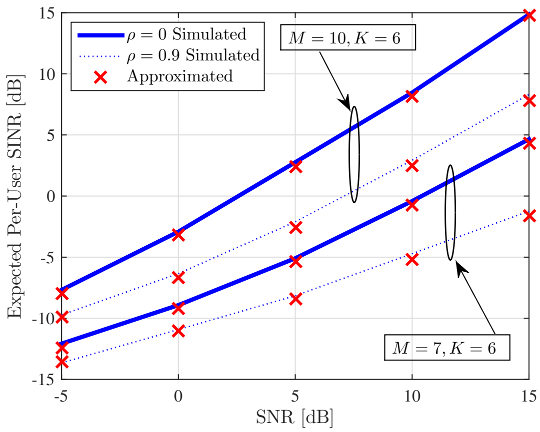

Fig. 1. Expected per-user SINR vs. SNR for $\rho = 0$ and 0.9.

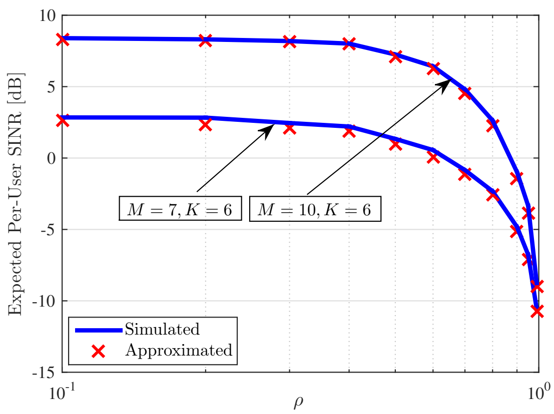

Fig. 2. Expected per-user SINR vs. ρ at SNR $= 10$ dB.

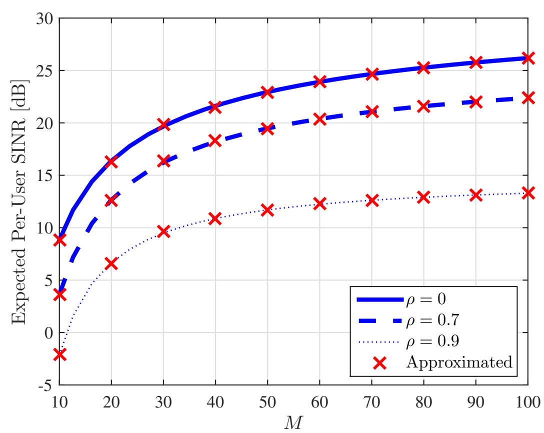

Fig. 3. Expected per-user SINR vs. M with fixed $K = 6$ at SNR $= 10$ dB.

are seen to remain tight with increasing M, consistent with Remark 2. Fig. 4 depicts the accuracy of Theorem 4, (with $M = 10$ and $K = 5$), where we see that at high SNR, with RZF converging to ZF, the instantaneous ZF per-user SNR very closely follows the gamma distribution for all values of ρ considered. Hence, not only can mean SINRs be provided, but precise distributional results in the high SNR regime can also be derived.

VI. Conclusion

The paper presents a general framework for the analysis of expected per-user SINR for MU-MIMO systems with RZF

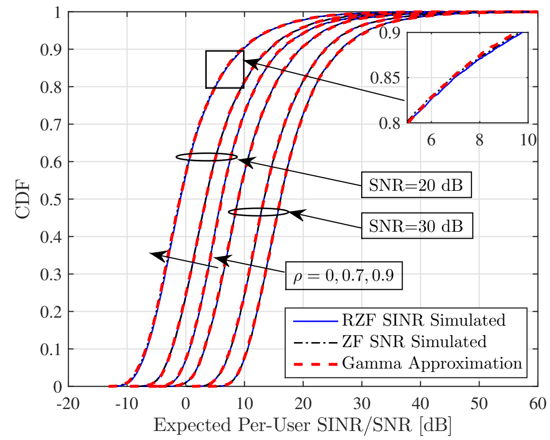

Fig. 4. Expected per-user SINR/SNR with a gamma distribution approximation at SNR $= 20, 30$ dB with $M = 10$ and $K = 5$.

precoding under spatially correlated Rayleigh fading channels. The analysis is robust to changes in system size, spatial correlation levels and SNRs in the system. Arbitrary eigenvalue densities of the complex Wishart channel correlation matrix are shown to be fundamental to the analysis. In deriving the expected SINR, we derive the joint density of two arbitrary eigenvalues for the complex Wishart matrix. In the high SNR regime, convergence of RZF to ZF was observed, and a distributional approximation to the instantaneous per-user SNR was introduced, where SNR was shown to closely follow the gamma distribution.

Appendix A
Proof of Theorem 1

$$\mathbb{E}_{\lambda}\left[\sum_{i=1}^{m}\left(\frac{\lambda_i}{\lambda_i+\xi}\right)^2\right] = m\left[\int_0^\infty \left(\frac{\lambda}{\lambda+\xi}\right)^2 f_0(\lambda)\, d\lambda\right], \quad (24)$$

where $f_0(\lambda)$ is the density of an arbitrary eigenvalue of $\boldsymbol{H}^{\mathrm{H}}\boldsymbol{H}$. Invoking Theorem 2 of [22], (24) becomes

$$mL\sum_{l=1}^{m}\sum_{\substack{j=1\\ j\neq l}}^{m}\mathcal{D}(l,j)\left[\int_0^\infty\left(\frac{\lambda}{\lambda+\xi}\right)^2\lambda^{j-1}\left(\theta_{n-m-l}^{n-m-1}e^{-\lambda/\theta_{n-m+l}}\right.\right.$$
$$\left.\left.-\sum_{p=1}^{n-m}\sum_{\substack{q=1\\ q\neq p}}^{n-m}\left[\boldsymbol{\Psi}^{-1}\right]_{q,p}\theta_{n-m+l}^{q-1}\theta_p^{n-m-1}e^{-\lambda/\theta_p}\right)d\lambda\right], \quad (25)$$

where the θ's are the eigenvalues of $\boldsymbol{R}$ and $L, \mathcal{D}(l,j), \boldsymbol{\Psi}$ are as defined in (9), respectively. After some trivial simplifications, (25) becomes

$$mL\sum_{l=1}^{m}\sum_{\substack{j=1\\ j\neq l}}^{m}\mathcal{D}(i,j)\left[\theta_{n-m+l}^{n-m-1}\int_0^\infty\frac{\lambda^{2+j-1}}{(\lambda+\xi)^2}e^{-\lambda/\theta_{n-m+l}}d\lambda-\sum_{p=1}^{n-m}\right.$$
$$\left.\sum_{\substack{q=1\\ q\neq p}}^{n-m}\left[\boldsymbol{\Psi}^{-1}\right]_{q,p}\theta_{n-m+l}^{q-1}\theta_p^{n-m-1}\int_0^\infty\frac{\lambda^{2+j-1}}{(\lambda+\xi)^2}e^{-\lambda/\theta_p}d\lambda\right]. \quad (26)$$

We recognize that the integrals in (26) have an identical form. Denoting $\bar{\mu} = 2 + j - 1$ and solving for the general case by substituting $\lambda = x - \xi$, we obtain

$$\Phi_2(a) = \int_0^\infty \frac{\lambda^{\bar{\mu}} e^{-\lambda/\theta_a}}{(\lambda+\xi)^2} d\lambda = \int_\xi^\infty \frac{(x-\xi)^{\bar{\mu}} e^{-(x-\xi)/\theta_a}}{(x)^2} dx$$
$$= \sum_{\gamma=0}^{\bar{\mu}} \binom{\bar{\mu}}{\gamma} (-\xi)^{\bar{\mu}-\gamma} e^{\xi/\theta_a} \int_\xi^\infty x^{\gamma-2} e^{-x} dx, \qquad (27)$$

where solution to the integral in (27) is given in (11). Substituting (27) into (26) and simplifying yields the desired expression in (8).

Appendix B
Proof of Theorem 2

We begin with the joint density of m distinct eigenvalues given by [17]

$$f(\lambda_1, \ldots, \lambda_m) = T \sum_\phi (-1)^{\mathrm{per}(\phi)} \prod_{i=1}^m \lambda_i^{\phi_i} \det(\boldsymbol{\Xi}), \qquad (28)$$

where T and $\boldsymbol{\Xi}$ are as defined in (13) and (14), respectively. Integrating over $\lambda_3, \ldots, \lambda_m$ in (28) yields,

$$f_0(\lambda_1, \lambda_2) = \frac{(n-2)!}{\prod_{j=1}^m j!} \sum_{i=0}^{m-1} \sum_{\substack{l=0 \\ l \neq i}}^{m-1} (-1)^{i+l-p(i,l)} \det(\boldsymbol{\Delta\Xi}_{il}), \qquad (29)$$

where $\boldsymbol{\Xi}_{il}$ is equivalent to $\boldsymbol{\Xi}$ with columns i and l ordered corresponding to λ_1 and λ_2 and $p(i,l)$ is as defined in (14). Performing a Laplace expansion on the i-th column with λ_1, we obtain (30). Performing a second Laplace expansion on the determinant in (29) with λ_2 and the j-th column yields the expression in Theorem 2.

Appendix C
Proof of Theorem 3

$$D_k = G_k^{(2)} + m(m-1) \int_0^\infty \int_0^\infty \left(\frac{\lambda_1}{\lambda_1+\xi}\right)\left(\frac{\lambda_2}{\lambda_2+\xi}\right)$$
$$f_0(\lambda_1, \lambda_2)\, d\lambda_2 d\lambda_1. \qquad (31)$$

Substituting the result from Theorem 2 and extracting the constants yields

$$D_k = G_k^{(2)} + m(m-1)\, T\, (n-2)! \sum_{i=0}^{m-1} \sum_{\substack{l=0 \\ l \neq i}}^{m-1} (-1)^{i+l-p(i,l)}$$
$$\sum_{o=1}^m \theta_o^{n-m-1} \sum_{\substack{p=1 \\ p \neq o}}^m (-1)^{p-p(o)} \boldsymbol{\Theta} \int_0^\infty \int_0^\infty \left(\frac{\lambda_1}{\lambda_1+\xi}\right)\left(\frac{\lambda_2}{\lambda_2+\xi}\right)$$
$$\lambda_1^i e^{-\lambda_1/\theta_o} \lambda_2^l e^{-\lambda_2/\theta_p} d\lambda_2\, d\lambda_1, \qquad (32)$$

where $p(o)$ and $\boldsymbol{\Theta}$ are as defined in (14), respectively.

Further simplification yields

$$D_k = G_k^{(2)} + m(m-1)\, T\, (n-2)! \sum_{i=0}^{m-1} \sum_{\substack{l=0 \\ l \neq i}}^{m-1} \sum_{o=1}^m \sum_{\substack{p=1 \\ p \neq o}}^m (-1)^{i+1-p(i,l)}$$
$$(-1)^{o-1} \theta_o^{n-m-1} (-1)^{p-p(o)} \boldsymbol{\Theta} \int_0^\infty \frac{\lambda_1^{i+1}}{\lambda_1+\xi} e^{-\lambda_1/\theta_o} d\lambda_1 \int_0^\infty \frac{\lambda_2^{l+1}}{\lambda_2+\xi}$$
$$e^{-\lambda_2/\theta_p} d\lambda_2. \qquad (33)$$

After recognizing that the integrals in (33) have identical form, we solve for the general case via change of variables where $\lambda = x - \xi$ and $\hat{\mu} = i + 1$, resulting in

$$\Phi_1(o) = \sum_{\gamma=0}^{\hat{\mu}} \binom{\hat{\mu}}{\gamma} (-\xi)^{\hat{\mu}-\gamma} e^{\xi/\theta_o} \int_\xi^\infty x^{\gamma-1} e^{-x} dx. \qquad (34)$$

The integral in (34) is a special case of the integral in (11). Likewise, by denoting $\hat{\mu} = l + 1$, we can evaluate $\Phi_1(p)$. Substituting $\Phi_1(o)$ and $\Phi_1(p)$ into (33) yields the desired expression in (15).

Appendix D
Proof of Theorem 4

Assuming that ω^{-1} is $\Gamma(\varrho, \chi)$, we observe that

$$\mathbb{E}\left[\omega^{-1}\right] = ((\varrho - 1)\chi)^{-1}, \qquad (35)$$

and

$$\mathrm{Var}\left[\omega^{-1}\right] = \left((\varrho-1)(\varrho-2)\chi^2\right)^{-1}. \qquad (36)$$

Re-arranging the equalities in (35) and (36) gives (23). Also, since $\omega = \sum_{i=1}^m \lambda_i^{-1}$, it is straight forward to show that

$$\mathbb{E}[\omega] = m\mathbb{E}\left[\lambda^{-1}\right], \qquad (37)$$

where λ is an arbitrary eigenvalue and

$$\mathbb{E}\left[\omega^2\right] = m\mathbb{E}\left[\lambda^{-2}\right] + m(m-1)\mathbb{E}\left[(\lambda_1, \lambda_2)^{-1}\right], \qquad (38)$$

where λ_1 and λ_2 are a pair of arbitrary eigenvalues. Hence (23) relies on $\mathbb{E}\left[\lambda^{-1}\right]$ and $\mathbb{E}\left[(\lambda_1\lambda_2)^{-1}\right]$, which are derived below.

We begin with (28) and integrate over $\lambda_2, \ldots, \lambda_m$. Upon reordering the columns of $\boldsymbol{\Xi}$, in the same way as in (29), we obtain

$$f(\lambda) = T(m-1)! \sum_{i=0}^{m-1} \det(\boldsymbol{\Delta\Xi}_i), \qquad (39)$$

where $\boldsymbol{\Xi}_i$ is the column corresponding to λ excluding the i-th entry. Thus,

$$\mathbb{E}\left[\frac{1}{\lambda}\right] = T(m-1)! \int_{\lambda=0}^\infty \left\{\left[\frac{\boldsymbol{\Xi}_o(\lambda)}{\lambda}\right] + \sum_{i=1}^{m-1}\left[\frac{\boldsymbol{\Xi}_i(\lambda)}{\lambda}\right]\right\} d\lambda, \qquad (40)$$

where

$$\boldsymbol{\Xi}_i(\lambda) = \sum_{j=1}^n (-1)^{n-m+i+j-1} \boldsymbol{\Xi}_{i,j} \theta_j^{n-m-1} e^{-\lambda/\theta_j}. \qquad (41)$$

When $i \geq 1$, we obtain

$$f_0(\lambda_1,\lambda_2)=\frac{(n-2)!}{\prod_{j=1}^{m} j!}\sum_{i=0}^{m-1}\sum_{\substack{l=0\\l\neq i}}^{m-1}(-1)^{i+l-p(i,l)}(-1)^{n-m}\sum_{o=1}^{m}(-1)^{o-1}\theta_o^{n-m-1}\lambda_1^i e^{-\lambda_1/\theta_o}\det\left(\mathbf{\Delta}_o\mathbf{\Xi}_{i,l;o}\right). \quad (30)$$

$$\int_0^\infty \frac{\Xi_i(\lambda)}{\lambda}d\lambda=\sum_{j=1}^{n}(-1)^{n-m+i+j-1}\,\Xi_{i,j}\theta_j^{n-m-1}\theta_j^i\,(i-1)!$$
$$=(i-1)!\sum_{j=1}^{n}(-1)^j\,\Xi_{i,j}\,(-\theta_j)^{n-m+i-1}. \quad (42)$$

Via substitution, it is straightforward to show that

$$\int_0^\infty \lambda_i e^{-\lambda/\theta}d\lambda=\int_0^\infty (v\theta)^i\,e^{-v}\theta\;dv=\theta^{i+1}\,i!. \quad (43)$$

When $i=0$,

$$\int_0^\infty \frac{\Xi_o(\lambda)}{\lambda}d\lambda=\lim_{\epsilon\to 0}\left\{\sum_{j=1}^{n}\kappa_j\mathrm{Ei}\left(1,\epsilon/\theta_j\right)\right\}, \quad (44)$$

where $\kappa_j=(-1)^{n-m+j-1}\,\Xi_{o,j}\theta_j^{n-m-1}$. Now as $\epsilon\to 0$, $\mathrm{Ei}\left(1,\epsilon/\theta_j\right)\approx c+\log_e\left(\epsilon/\theta_j\right)=c+\log_e(\epsilon)-\log_e(\theta_j)$, where c is an arbitrary constant. This yields

$$\int_0^\infty \frac{\Xi_o(\lambda)}{\lambda}d\lambda=\sum_{j=1}^{n}(-1)^{n-m+j}\,\Xi_{o,j}\theta_j^{n-m-1}\log_e(\theta_j), \quad (45)$$

since $\sum_{j=1}^{n}\kappa_j=0$. This follows from the fact that

$$\det(\mathbf{\Delta\Xi})=\sum_{j=1}^{n}(-1)^{n-m+j-1}\,\theta_j^{n-m-1}\Xi_{o,j}=\sum_{i=1}^{n}\kappa_j=c, \quad (46)$$

since $\mathbf{\Delta\Xi}$ has two equal columns in $n-m$ and $n-m+1$ and therefore has zero determinant. Combining the above results gives

$$\mathbb{E}\left[\frac{1}{\lambda}\right]=T\,(n-1)!\left\{\sum_{j=1}^{n}(-1)^{n-m+j}\,\Xi_{o,j}\theta_j^{n-m-1}\log_e(\theta_j)+\right.$$
$$\left.\sum_{i=1}^{m-1}(i-1)!\sum_{j=1}^{n}(-1)^j\,\Xi_{i,j}\,(-\theta_j)^{n-m+i-1}\right\}. \quad (47)$$

Similarly, integrating the density in (28) over $\lambda_3,\ldots,\lambda_k$ and following the above steps yields

$$\mathbb{E}\left[\frac{1}{\lambda_1\lambda_2}\right]=2T\,(n-2)!\left\{\sum_{l=1}^{n}(-1)^{n-m+l}\,\mathrm{Ei}_{lj}\theta_l^{n-m-1}\right.$$
$$\left.\log_e(\theta_k)+\sum_{i=1}^{m-1}\sum_{\substack{j=1\\j\neq i}}^{m-1}\Xi_{i,j}\right\}. \quad (48)$$

References

[1] T. Marzetta, "Noncooperative cellular wireless with unlimited numbers of base station antennas," *IEEE Trans. Wireless Commun.*, vol. 9, no. 11, pp. 3590–3600, Nov. 2010.

[2] D. Gesbert, M. Shafi, D. Shiu, P. Smith, and A. Naguib, "From theory to practice: An overview of MIMO space-time coded wireless systems," *IEEE J. Sel. Areas Commun.*, vol. 21, no. 3, pp. 281–302, Apr. 2003.

[3] T. Yoo and A. Goldsmith, "On the optimality of multiantenna broadcast scheduling using zero-forcing beamforming," *IEEE J. Sel. Areas Commun.*, vol. 24, no. 3, pp. 528–541, Mar. 2006.

[4] C. B. Peel, B. M. Hochwald, and A. L. Swindlehurst, "A vector-perturbation technique for near-capacity multiantenna multiuser communication-part I: Channel inversion and regularization," *IEEE Trans. Commun.*, vol. 53, no. 1, pp. 195–202, Jan. 2005.

[5] X. Gao, O. Edfors, F. Rusek, and F. Tufvesson, "Linear pre-coding performance in measured very-large MIMO channels," in *Proc. IEEE Veh. Techol. Conf. (VTC) Fall*, Sept. 2011, pp. 1–5.

[6] C. Masouros, M. Sellathurai, and T. Ratnarajah, "Large-scale MIMO transmitters in fixed physical spaces: The effect of transmit correlation and mutual coupling," *IEEE Trans. Commun.*, vol. 61, no. 7, pp. 2794–2804, Jul. 2013.

[7] Z. Lin, T. Sorensen, and P. Mogensen, "Downlink SINR distribution of linearly precoded multiuser MIMO systems," *IEEE Commun. Lett.*, vol. 11, no. 11, pp. 850–852, Nov. 2007.

[8] J. Fan, Z. Xu, and G. Li, "Performance analysis of MU-MIMO in downlink cellular networks," *IEEE Commun. Lett.*, vol. 19, no. 2, pp. 223–226, Feb. 2015.

[9] J. Hoydis, S. ten Brink, and M. Debbah, "Massive MIMO in the UL/DL of cellular networks: How many antennas do we need?" *IEEE J. Sel. Areas Commun.*, vol. 31, no. 2, pp. 160–171, Feb. 2013.

[10] D. Wang, C. Ji, X. Gao, S. Sun, and X. You, "Uplink sum-rate analysis of multi-cell multi-user massive MIMO system," in *Proc. IEEE Int. Conf. on Commun. (ICC)*, Jun. 2013, pp. 5404–5408.

[11] H. Bahrami and T. Le-Ngoc, "Precoder design based on the channel correlation matrices," *IEEE Trans. Wireless Commun.*, vol. 5, no. 12, pp. 3579–2587, Dec. 2006.

[12] J. Akhtar and D. Gesbert, "Spatial multiplexing over correlated MIMO channels with a closed-form precoder," *IEEE Trans. Wireless Commun.*, vol. 4, no. 5, pp. 2400–2409, Sept. 2005.

[13] J. Hoydis, S. ten Brink, and M. Debbah, "Comparison of linear precoding schemes for downlink massive MIMO," in *Proc. IEEE Int. Conf. on Commun. (ICC)*, Jun. 2012, pp. 2135–2139.

[14] D. Nguyen and T. Le-Ngoc, "MMSE precoding for multiuser MISO downlink transmission with non-homogeneous user SNR conditions," *EURASIP Journal on Adv. Signal Process.*, vol. 85, no. 1, pp. 1–12, Jun. 2014.

[15] A. Goldsmith, *Wireless Communications*, 2nd ed. Cambridge University Press, 2005.

[16] L. Yu, W. Yiu, and R. Langley, "SINR analysis of the subtraction-based SMI beamformer," *IEEE Trans. Signal Process.*, vol. 58, no. 11, pp. 5926–5932, November 2010.

[17] P. Smith, S. Roy, and M. Shafi, "Capacity of MIMO systems with semicorrelated flat fading," *IEEE Trans. Inf. Theory.*, vol. 49, no. 10, pp. 2781–2788, Oct. 2003.

[18] H. Tataria, P. Smith, M. Shafi, and P. Dmochowski, "Generalized analysis of coordinated regularized zero-forcing precoding: An application to two-tier small cell networks," *submitted to IEEE Trans. Wireless Commun.*, 2015.

[19] H. Tataria, P. Smith, L. Greenstein, P. Dmochowski, and M. Shafi, "Performance and analysis of downlink multiuser MIMO systems with regularized zero-forcing precoding in Ricean fading channels," *in Proc. of IEEE Int. Conf. on Commun. (ICC)*, 2016.

[20] D. Gore, R. Heath, and A. Paulraj, "Transmit selection in spatial multiplexing systems," *IEEE Commun. Lett.*, vol. 6, no. 11, pp. 491–493, Nov. 2002.

[21] S. L. Loyka, "Channel capacity of MIMO architecture using the exponential correlation matrix," *IEEE Commun. Lett.*, vol. 5, no. 9, pp. 369–371, September 2001.

[22] G. Alfano, A. Tulino, A. Lozano, and S. Verdu, "Capacity of MIMO channels with one-sided correlation," in *Proc. IEEE Eighth Intl. Symp. on Spread Spectrum Tech. and App.*, Aug 2004, pp. 515–519.